

2.B Absorption Spectroscopy as a Diagnostic for Highly Compressed Targets

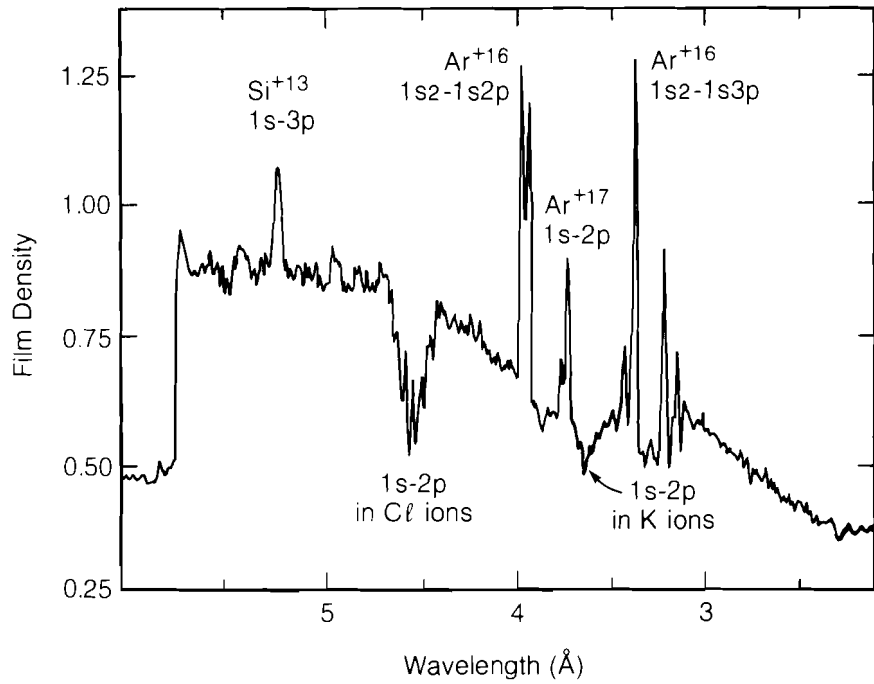
This article examines the possibility of using absorption spectroscopy as a compression diagnostic for high-density implosion experiments. Such experiments, planned for the 24-beam OMEGA UV laser, are of two kinds: (1) gas-filled targets designed to exceed compressions of 50 times liquid DT density, and (2) cryogenic fuel targets designed to exceed 200 times liquid DT density.¹ Some results for diagnosing the cryogenic targets are presented here.

Emission-line spectroscopy of fuel additives is not expected to be a suitable diagnostic for these high-compression experiments for several reasons. In glass-shell targets overcoated with plastic, the compressed glass shell significantly blocks emission lines from low-Z fuel additives (up to \sim argon, $Z = 18$). If the fuel is seeded with higher-Z elements, the attenuation would be sufficiently low for resonance line emission from the most highly ionized species, but the low central temperatures required for high compression may not be adequate to produce these states of ionization in sufficient abundance. In addition, radiation by fuel additives can modify the implosion by cooling the compressed DT, so that the resulting compression is not indicative of the compression attainable with the same target filled with pure DT. It may in fact be impossible to fabricate cryogenic targets with fuel additives, since any impurities would condense out of the DT gas and freeze against the inner wall of the shell before the DT condenses.

With absorption spectroscopy, one measures the areal density (ρR) of the target shell using absorption features that have been impressed upon continuum radiation as it passes through the shell. The $1s-2p$ absorption transition in helium-like through fluorine-like ions form absorption lines whose total strength is nearly proportional to ρR of the absorbing material.² Such lines have been observed in KCl shell ions in implosion experiments at the Los Alamos National Laboratory (LANL) (see Fig. 24.7)² and have been observed in silicon ions from ablative implosions performed at LLE.³ These absorption lines provide a spectral signal, at relatively high photon energies (a few keV), from ions in a relatively cool ($T_e \sim \text{few} \times 100$ eV) environment. The continuum-absorption processes can also shape the emission continuum in a ρR -dependent fashion.

The usefulness of these absorption effects are examined using non-LTE simulations of spectra calculated with an atomic rate-equation radiative-transfer code, together with 1-D hydrocode (*LILAC*) calculations of the high-compression implosions. The absorption features are examined for several variations of the same target. The simulated spectra show roughly what diagnostic capabilities are required, including temporal resolution, spatial resolution, and sensitivity.

In obtaining the spectrum simulations, atomic populations for all ionization species are calculated by solving time-dependent rate equations. The populations are used to calculate non-LTE opacities and



E3295

*Courtesy of A. Hauer, LANL

Fig. 24.7
Absorption lines due to a KCl layer in a CO₂-laser-imploded target consisting of a glass shell with KCl and CH coatings and a DT-plus-argon (1%) fill. This figure was provided by Allan Hauer of LANL.²

emissivities, and the resultant radiation is transported out of the target. Simple analytic expressions for the atomic energies and rates are used, many based on the screened-nucleus hydrogenic-ion model that includes tabulated line profiles and continuum lowering.⁴ Distinct excited-state populations are calculated for the hydrogen-like and helium-like species, and only ground-state populations are kept for each remaining degree of ionization.

The determination of the shell ρR from absorption lines is based on the photoexcitation cross section per unit frequency interval

$$\sigma_\nu = \sigma L(\nu), \tag{1}$$

where σ is the total cross section

$$\sigma = (\pi e^2/mc)f, \tag{2}$$

f is the absorption oscillator strength, and $L(\nu)$ is the normalized line profile

$$\int L(\nu)d\nu = 1. \tag{3}$$

The attenuation of intensity I_0 passing through the shell is given in terms of the shell ρR by

$$I(\nu) = I_0 \exp(-\alpha\sigma_\nu\rho R/M_i), \tag{4}$$

where α is the fraction of all ions in the absorbing state and M_i is the mean ion mass. The ρR is then given by

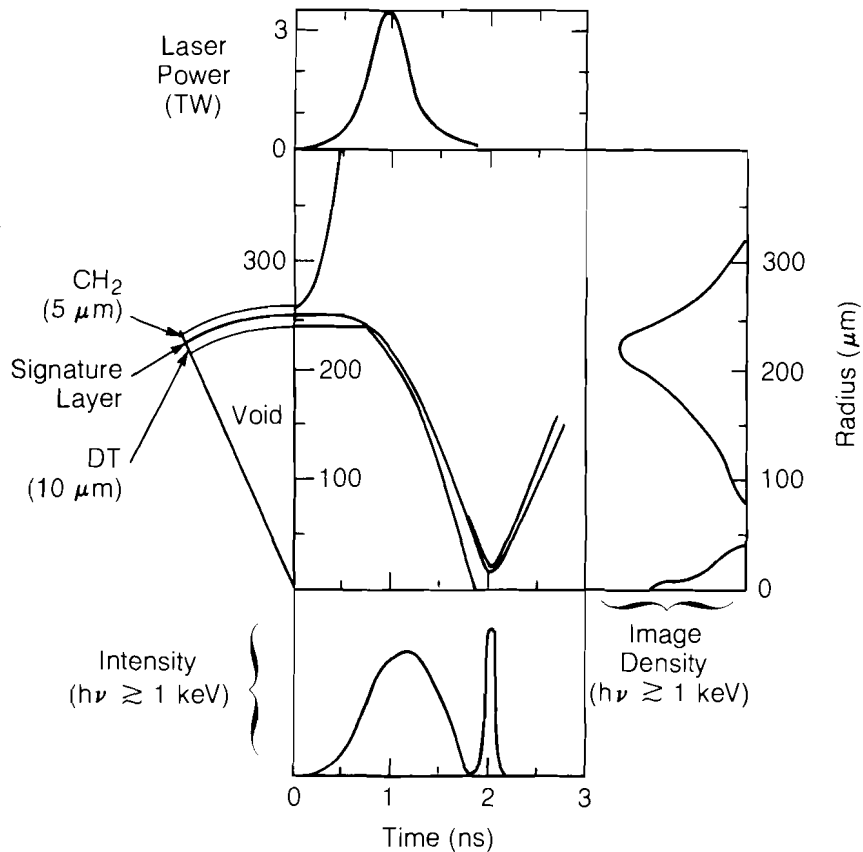
$$\rho R = (M_i/\alpha\sigma) \int \ell n [I_0/I(\nu)] d\nu. \quad (5)$$

If the instrument response is logarithmic, then the integral is simply the area within the line, below the background continuum level. Note that the integration in Eq. (5) [together with Eq. (3)] eliminates the line profile $L(\nu)$ from the determination of ρR . Non-LTE computer simulations can be useful in interpreting experimental spectra when complications such as foreground emission must be taken into account or when estimates of the size and the spatial and temporal extent of the absorbing species are needed.

Fig. 24.8
The layer-boundary trajectories of a representative high-compression target imploded by a 2-kJ pulse. The total hard x-ray emission from this implosion is plotted as both a time-resolved and spatially resolved signal against the radius and time axes of the layer-boundary trajectory plot.

Results of Computer Simulations

A representative cryogenic target is shown in Fig. 24.8. It consists of a cryogenic DT layer inside a CH₂ shell, with the option of using a middle layer of glass. The calculated fuel compression exceeds 200 times liquid density when imploded by the 2-kJ pulse shown. The



TC1671

bottom plot of x-ray emission (> 1 keV) versus time shows a distinct separation of about 100 to 200 ps between the emission from the laser-heated ablation region in the CH_2 layer and from the core at peak compression. All the spectra from cryogenic targets shown in this article will be time integrated over the compression peak. Experimentally, this assumes a time-resolution capability of rejecting the ablator emission up to about 200 ps before the compression emission begins. As can be seen in the plot of time-integrated, spatially resolved emission at the far right of the figure, the compression emission can also be isolated by masking the image with a circular aperture roughly 60 to 100 μm in diameter. The glass shell can be doped with an additive to produce the desired absorption lines, or it can be replaced entirely with another signature layer.

The first signature layer to be considered is 1- μm thick, consisting of glass mixed with a 1% calcium impurity (all concentrations in this article are given by atom percent). Calcium is often a naturally occurring impurity in glass. The temperature and density profiles in this layer at peak compression are shown in Fig. 24.9 and are sufficient to ionize the

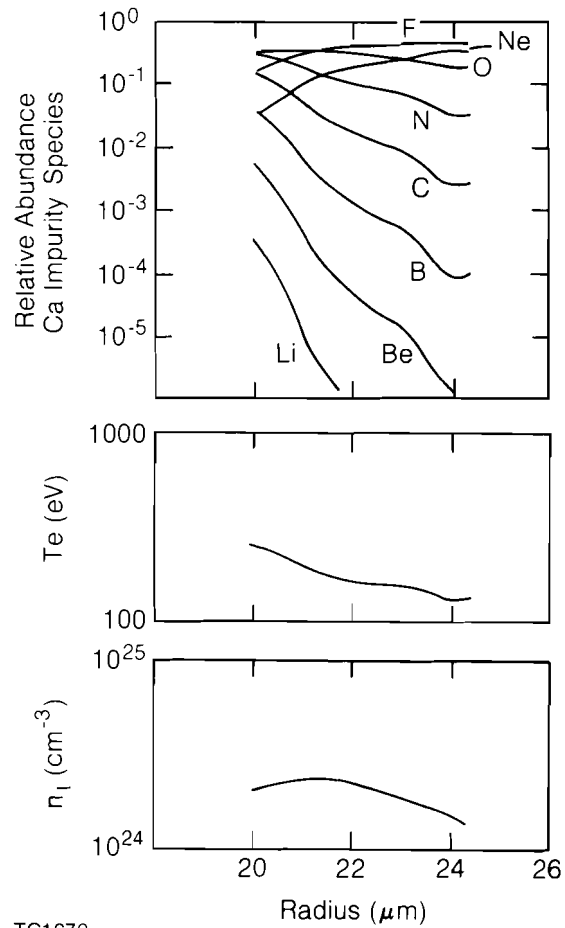


Fig. 24.9
Conditions in the glass shell at peak compression of a cryogenic target.

calcium impurity to beyond the fluorine-like species. The absorption lines from the 1s-2p transition are formed by all species from fluorine-like through helium-like. For calcium, these transitions occur at energies sufficiently high (3.7-3.9 keV) that the line absorption is not obscured by continuum emission in the glass.

The 1s-2p absorption transition is illustrated in Fig. 24.10 in the context of the simple atomic model used in the simulation. The two examples are the helium-like and boron-like species. The transition energies for each species and for each initial configuration of the n=2 shell are nearly the same because the electron orbits are only slightly perturbed by adding electrons to the n=2 shell. For the case of calcium, the shift in transition energy is only about 25 eV between successive species.⁵ This small shift suggests that the initial and final electron orbits are fairly similar from species to species and that the transition matrix elements likewise ought not to change by a large

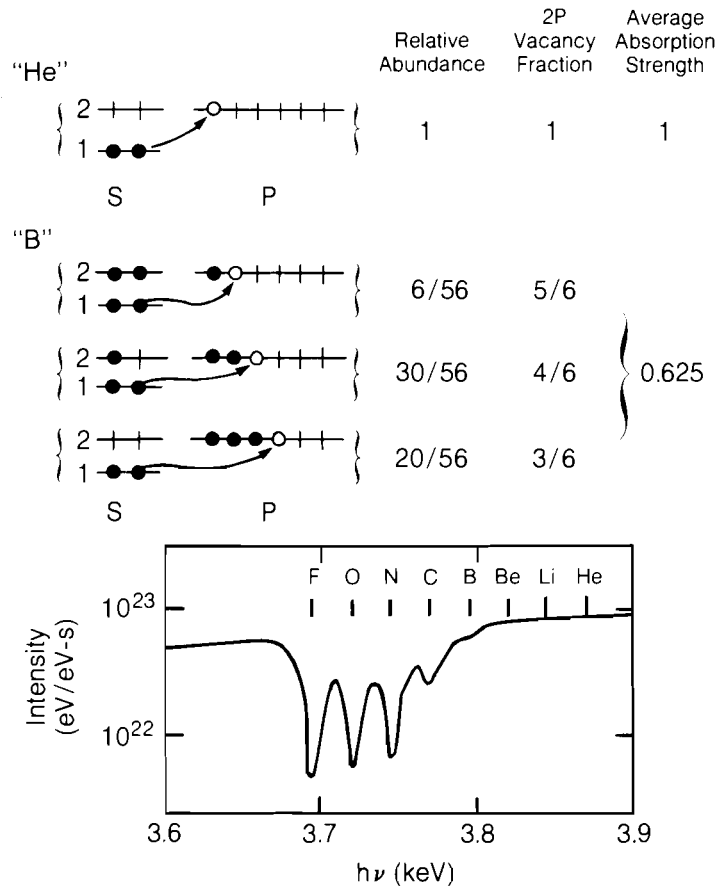


Fig. 24.10
An illustration of the K-shell (1s-2p) process that forms the series of absorption lines for the proposed diagnostic. The inset is a detail of the spectral intensity from the glass-shell target at the point in time depicted in Fig. 24.9.

TC1673

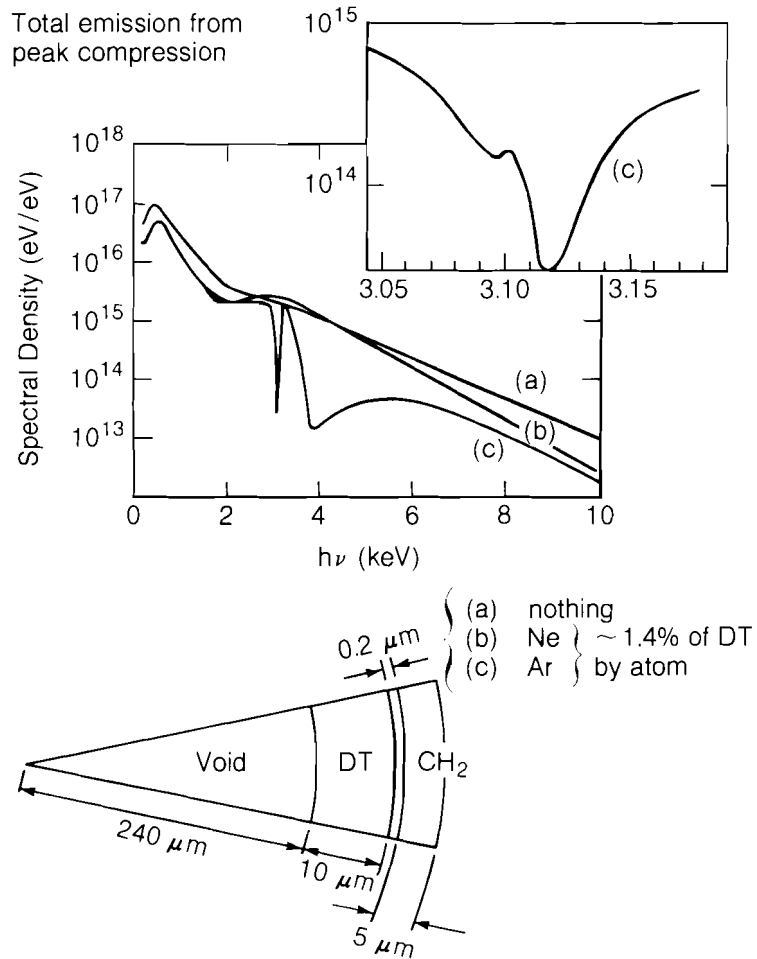
amount. The approximation used is that the absorption cross section for each species is the cross section for the helium-like species with a factor accounting for the reduced vacancy fraction of the 2p shell as it fills. The cross section of each species is a statistically weighted average over the possible partitionings of $n=2$ electrons among the 2s and 2p shells in the initial state. In the simple atomic model used, the 2s and 2p levels are treated as degenerate. In reality, the 2s shell is filled first because of its lower energy, leaving the 2p shell more open, so the average cross section for each species is slightly larger than the average used here. As a consequence, the approximation used underestimates the intensity of the absorption line and is, in this one respect, conservative. For the example of the boron-like species, one can average the 2p-shell vacancy fractions over the relative statistical weights given for the respective initial configurations. The result is that the average 2p vacancy fraction is 0.625, so that the average absorption strength per ion for that species is 0.625 relative to the absorption strength for the helium-like species.

The spectrum at the bottom of Fig. 24.10 is the simulated spectral intensity for the glass-shell target at the time depicted in Fig. 24.9. The intensities of the absorption lines reflect the relative abundances of the corresponding species. Due to limitations in the current version of the simulation code, the absorption lines for each species will be superimposed at the same line energy using the helium-like line profile in all the simulations to follow. Even though the multiple-component structure will not be depicted, the total 1s-2p absorption due to all species will be accurately represented.

As a second example, we consider layers of argon and neon, condensed out of the fill gas against the inner-shell surface of a cryogenic target. They show the same absorption transition as the calcium impurity in the glass shell, but the shell transparency gained by removing the glass gives a much stronger signal. Figure 24.11 shows the initial configuration of the target with the glass-free signature layer. Spectra obtained assuming neon and argon fuel additives are compared with the spectrum obtained for a target with no signature layer. While the argon absorption line is very distinct, the neon absorption line is at a low enough energy to be blocked by the continuum opacity of the CH_2 shell.

For the purpose of this article, a time-integrated spectral intensity of 10^{13} can be taken as a state-of-the-art threshold sensitivity, with 10^{14} being a level where the shape of the spectrum can be seen. Such thresholds are difficult to estimate, and they do not anticipate future improvements in sensitivity. Possible approaches to improved sensitivity may involve large dispersing crystals in focusing geometries, such as in the von Hamos geometry.⁶

Another example of a glass-free shell is illustrated in Fig. 24.12. The spectrum is from a target with a KCl signature layer placed within the CH_2 shell. Absorption lines from both potassium and chlorine are seen. For comparison, the bottom spectrum from the glass-shell target shows the calcium absorption line at a very low intensity. At present, this particular glass-shell target is probably not diagnosable with x rays,



TC1674

Fig. 24.11
Effects of fuel additives on the spectrum of a cryogenic target.

unless it does not perform as predicted by 1-D hydrodynamic simulations.

The minimum of the glass-shell intensity—near 3 keV—occurs at the energy at which the bound-free optical depth of the glass becomes small enough to allow the harder continuum from the DT to appear over the optically thick continuum of the cooler glass. The position of this minimum is another indication of the ρR of the glass shell. At the same time that the optical thickness of the glass obscures the absorption line, it provides, at least in principle, another absorption feature that is sensitive to the ρR of the shell.

The simulation of the glass-shell implosion was repeated with lower laser power in order to show how the absorption features change as the fuel and shell compressions are reduced. The resulting peak ρR values for these simulations are tabulated in Fig. 24.13. The corresponding spectra show that the point of inflection of the transmitted continuum

moves from 3 keV toward lower energies as the ρR of the shell decreases. At the lowest shell compression, the shell is thin enough to allow the K-edge and line absorption of silicon to appear. The total strength of the calcium line decreases with the shell ρR , and the profile of the line narrows as the peak density of the shell decreases. These trends can be explained qualitatively in terms of changes in the shell conditions at peak compression, but this perspective is somewhat oversimplified since the spectra are records covering hundreds of picoseconds, during which the target conditions are changing rapidly.

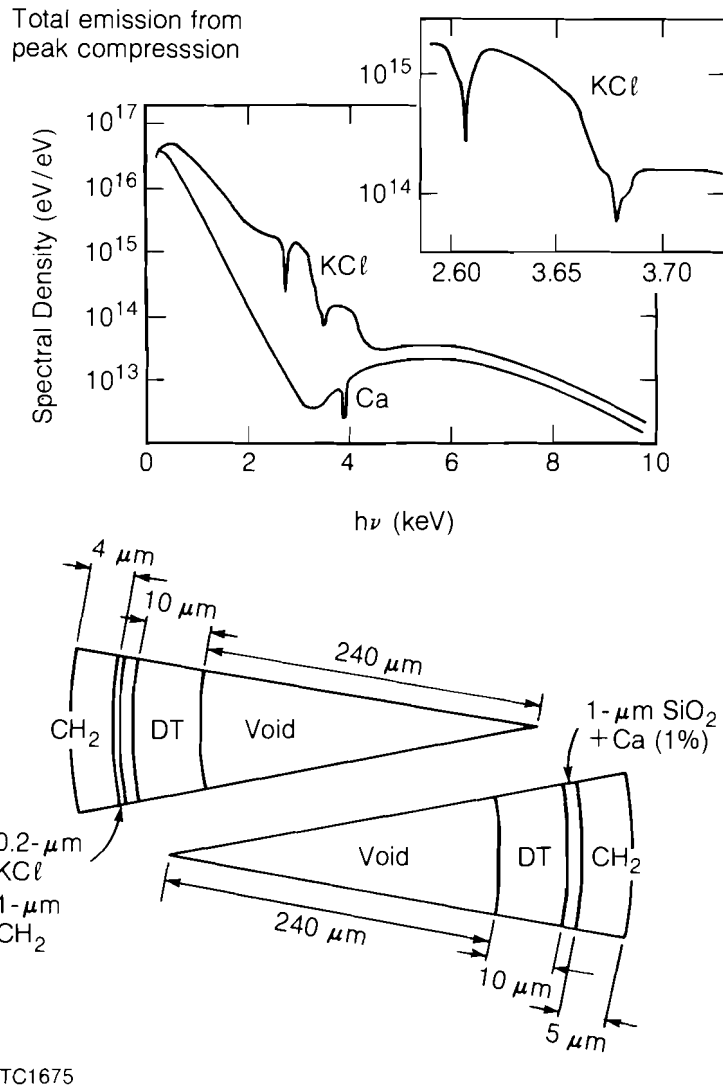
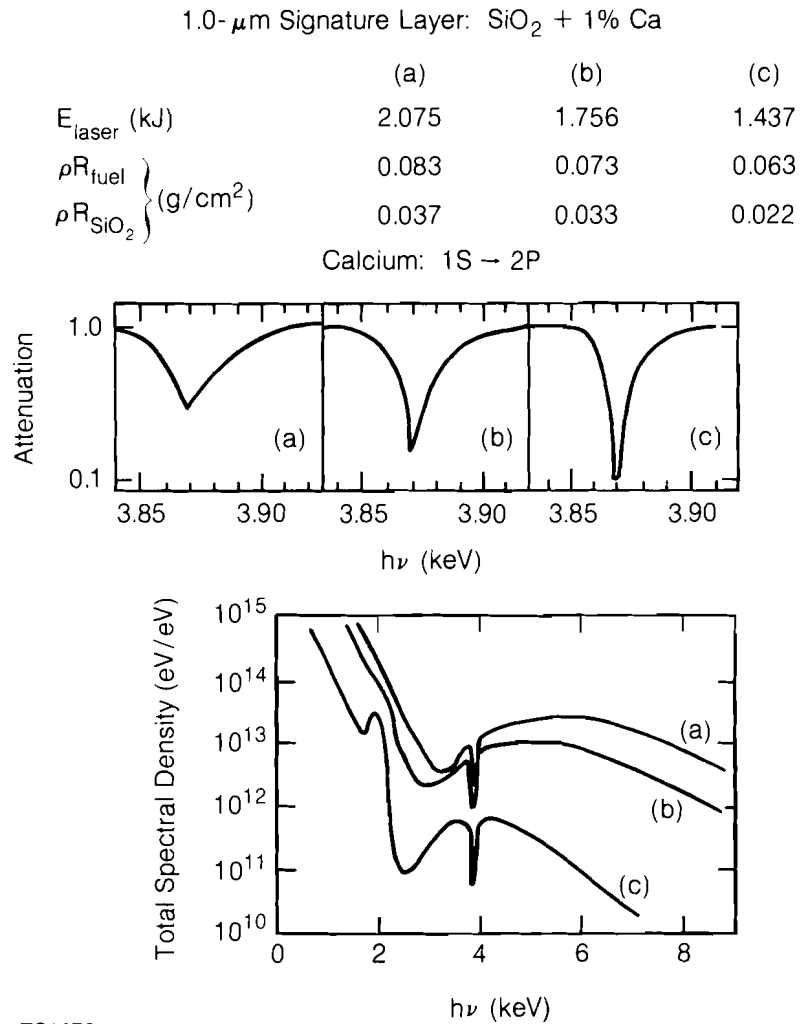


Fig. 24.12
Increased intensity with glass-free shells.



TC1676

Fig. 24.13
Dependence of absorption features on target performance.

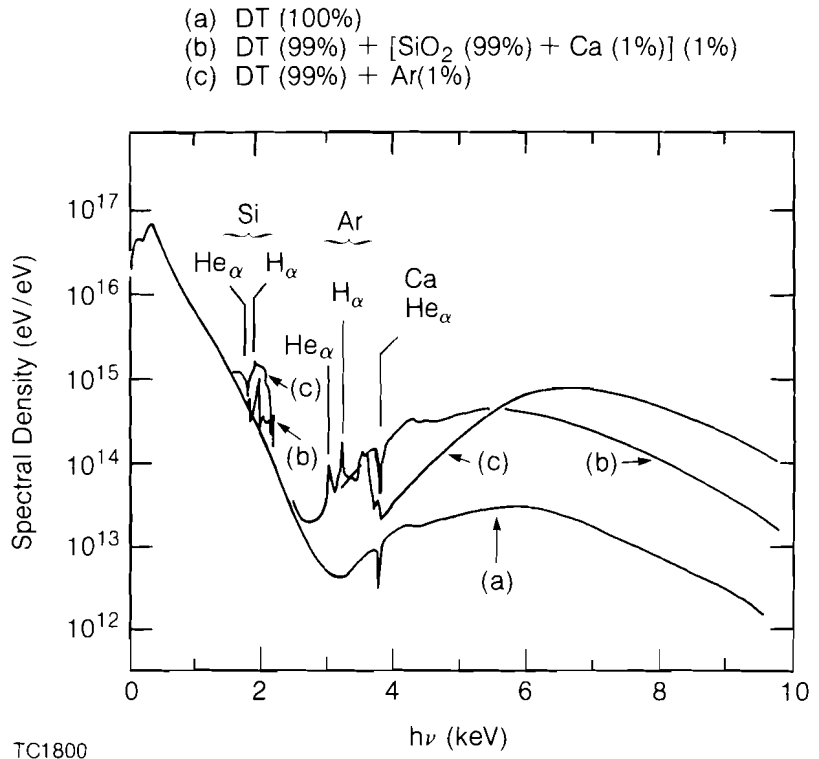
Mixing

In actual experiments, the targets considered here will not implode in the purely spherical mode of 1-D simulations. A combination of the nonuniformities in the laser illumination of the target and the Rayleigh-Taylor instability of the decelerating shell prior to peak compression may cause the shell to break up, resulting in compression conditions different from those predicted.¹ In the spherical simulations shown previously, the shell material remains relatively cool ($T_e \leq 200$ eV). If high-Z material from the disrupted shell mixes with DT that is heated to temperatures close to the predicted peak temperatures ($T_e \leq 1$ keV), then emission lines may appear as evidence that disruption has taken place.

The spectral signature of mixing has been obtained approximately by adding shell material to the DT as part of the initial conditions of the spectrum simulation. The same hydrocode information is used for this simulation as for the simulation without mixing so that the change of chemical composition is the only mixing effect modeled. At present, the non-LTE spectrum simulation can be performed only on 1-D simulations, which cannot model the hydrodynamics of mixing and the resulting time-dependent impurity concentrations.

Emission lines from shell material mixed into the hot DT must be of sufficient energy to penetrate the remaining intact shell. In the glass-free examples, lines from the hydrogen-like and helium-like species of argon, potassium, or chlorine in the DT penetrate the shell, but neon lines do not, unless the shell is severely thinned by hydrodynamic breakup. Simulations of the glass-shell target were obtained with the DT contaminated at a level of 1% by atom with shell material. The results are shown in Fig. 24.14. Curve (b) is obtained for the DT-shell mixture, which is to be compared with curve (a) obtained for a pure DT fill. Silicon features are seen at energies below the K-edge, where the glass shell is relatively transparent. Silicon $H\alpha$ is emitted, and the $He\alpha$ line is seen weakly in absorption. The shell transparency to these silicon features is marginal. In fact, the simulation shows that these features are blocked for about 150 ps, around the time of peak compression, when the ρR of the glass shell is above 0.02 g/cm² (peak $\rho R = 0.037$ g/cm²). These silicon features are very sensitive to the atomic

Fig. 24.14
Appearance of emission lines with fuel (DT) additives.



modeling. The same simulation performed with tabulated LTE opacities⁷ for the glass shell shows no penetration of the shell by silicon lines. This can be explained with only a factor-of-two increase in the calculated opacity.

Curve (c) in Fig. 24.14 was obtained for an argon contaminant. The high-energy continuum is strongly enhanced, as in the shell-contaminated case. Argon 1s-2p lines are seen, although the glass attenuates them a great deal. The line-like structure near 4 keV is in part due to the superposition of ionization edges acting in emission and absorption. The line-like sharpness of these edges is an artifact of the uniformly layered structure of the target and of the simplified atomic model, which uses only a few ionization transitions to model ionic spectra.

The emission features in Fig. 24.14 are sensitive to the mixing depth. The temperatures in the spherical simulations are peaked in the center, and the emission features are not obtained if the contaminants are confined to the outer half of the fuel mass.

This discussion of mixing is necessarily preliminary because the spectrum simulations are based on ideally behaved implosion simulations with constant impurity concentrations. The development of diagnostics to detect shell disruption and other failure modes is an important goal that will require simulation studies using more realistic mixing models than the very simple one used here.

ACKNOWLEDGMENT

This work was supported by the U.S. Department of Energy Office of Inertial Fusion under agreement number DE-FC08-85DP40200 and by the Laser Fusion Feasibility Project at the Laboratory for Laser Energetics which has the following sponsors: Empire State Electric Energy Research Corporation, General Electric Company, New York State Energy Research and Development Authority, Northeast Utilities Service Company, Ontario Hydro, Southern California Edison Company, The Standard Oil Company, and University of Rochester. Such support does not imply endorsement of the content by any of the above parties.

REFERENCES

1. P. McKenty and C. P. Verdon, LLE Theory Group Report No. 15, 1985.
2. A. Hauer *et al.* (paper in preparation); LLE Review **22**, 51 (1985).
3. B. Yaakobi, R. L. McCrory, S. Skupsky, J. A. Delettrez, P. Bourke, H. Deckman, C. F. Hooper, and J. M. Soures, *Opt. Commun.* **34**, 213 (1980).
4. S. Skupsky, LLE Theory Group Report No. 11, 1979; R. Epstein, LLE Theory Group Report No. 13, 1984; R. Epstein, S. Skupsky, and J. Delettrez, *J. Quant. Spectrosc. Radiat. Transfer* (to be published).
5. L. L. House, *Astrophys. J. Suppl. Ser.* **18**, 21 (1969).
6. B. Yaakobi, R. E. Turner, H. W. Schnopper, and P. O. Taylor, *Rev. Sci. Instrum.* **50**, 1609 (1979).
7. W. F. Huebner, A. L. Merts, N. H. Magee, and M. F. Argo, Report No. LA-6760, 1977 (unpublished).